Solid-State Electronics 200 (2023) 108542

Contents lists available at ScienceDirect

Solid State Electronics

journal homepage: www.elsevier.com/locate/sse

Coupling a phase field model with an electro-thermal solver to simulate PCM intermediate resistance states for neuromorphic computing☆

O. Cueto *, A. Trabelsi, C. Cagli, M.C. Cyrille

Univ. Grenoble Alpes, CEA, LETI, F-38000 Grenoble, France

ARTICLE INFO

Keywords:
Neuromorphic computing
PCM
Resistance states
Progressive crystallization
Simulation
Phase field model

ABSTRACT

A key attribute for Phase-Change Memories to be used for neuromorphic computing is the possibility to create intermediate resistance states by the progressive crystallization during the successive application of set pulses. To complete an experimental approach, we studied progressive crystallization by simulation. Insight on the real mechanisms of progressive crystallization is obtained by coupling Joule heating, diffusion of heat and a phase change model relying on the Phase Field Method.

1. Introduction

Phase-Change Memories (PCM) are today considered the most mature among novel non-volatile memory technologies. PCM rely on the reversible and rapid phase transition between the amorphous and crystalline phases of chalcogenide materials such as Ge2Sb2Te5 (GST225). The ability to alter the conductance levels in a controllable way makes PCM devices particularly well-suited for synaptic realizations in neuromorphic computing [1–3]. The PCM devices are currently being investigated as building blocks for neuromorphic circuits [4]. A key attribute that enables this application is the progressive crystallization of the phase-change material and subsequent increase in device conductance by the successive application of appropriate electrical pulses. We studied by simulation the progressive crystallization of GST225 PCM with a dedicated tool relying on the Phase Field Method (PFM) coupled with an electro-thermal solver [5]. The devices studied are GST225 state-of-the-art PCM devices. The simulations presented in this work were compared to electrical results relative to conductance evolution during progressive application of recrystallization pulses. Our model allows understanding the mechanisms of recrystallization during set pulses and consequently can help controlling the intermediate states of resistance of PCM devices.

2. A solver for PCM coupling the Phase-Field method with an electro-thermal model

The Phase-Field Method (PFM) is a continuum model based on non equilibrium thermodynamics used in materials science to simulate the evolution of microstructures [6,7]. The PFM method can be extended to take into crystalline grains orientation [8]. This method is now widely used in phase change problems and failure process problems [9–12]. The finite element electro-thermal solver coupled with the Phase Field Method was already presented [5] and we just give here a reminder of its main features. The PFM relies on an order parameter η representing the local crystallinity of PCM material ($\eta = 1$ in the crystalline phase and $\eta = 0$ in amorphous phase). Time evolution of η is governed by the Allen–Cahn Eq. (1) and corresponds to the reduction of the total energy of the system composed of free-energy of bulk phases and energy of interfaces between phases [13].

$$\frac{\partial \eta}{\partial t} = -L_\eta \left(\frac{\partial f(\eta, T)}{\partial \eta} - \kappa \nabla^2 \eta \right) \tag{1}$$

$f(\eta, T)$ is a local free-energy density for which we use the expression proposed by [14]. L_η is a positive kinetic coefficient, $f(\eta, T)$ is a local free-energy density that consists of a double well function f_{dw} and an interpolation function $f_p(\eta, T)$.

At the melting point, the two phases have the same free energy density and there is no driving force for crystallization but the two phases are separated by a free energy barrier represented by the double-well potential.

The kinetic coefficient L_η, introduced in Eq. (1), can be calculated from the front velocity (which in our case is the crystalline growth velocity V_g) by the equality:

$$L_\eta = \frac{V_g \cdot R_c}{\kappa} \tag{2}$$

☆ The review of this paper was arranged by Francisco Gamiz.

* Corresponding author.
E-mail address: olga.cueto@cea.fr (O. Cueto).

https://doi.org/10.1016/j.sse.2022.108542

Available online 25 November 2022

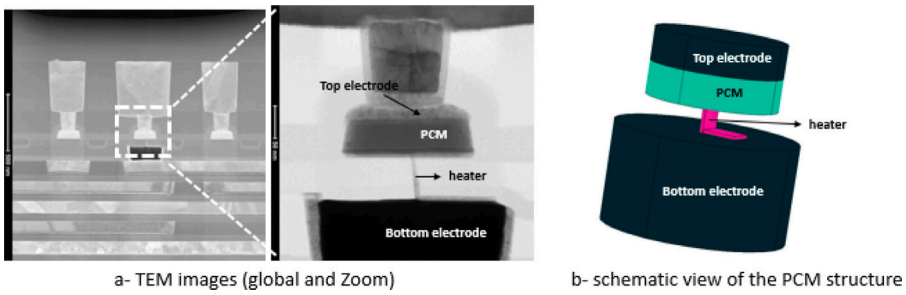

a- TEM images (global and Zoom) b- schematic view of the PCM structure

Fig. 1. Illustration of the PCM device.

where R_c is the curvature radius of the interface that we will consider as equal to the radius of critical nuclei [13,14]. Main thermodynamical parameters are given in [5]. The parameters of the PFM method, κ and H, are considered constant for this work.

Phase change mechanisms that occur during the PCM operations generally involve concurrent nucleation and growth. Nucleation could be introduced in the PFM as an additional Langevin noise term in Eq. (1) but this can become computationally expensive since it requires sampling at a very high frequency if nucleation events are very rare. In our work, nucleation model is maintained as a separate entity from the Phase-Field equation: we use two algorithms which alternate, one for nucleation and one for growth and coarsening corresponding to the advance of Eq. (1).

Our nucleation model relies on the classical nucleation theory. Due to the very fast increase (in the order of 10^{12} K/s) and decrease of temperature (in the order of 10^{10} K/s) associated to the electrical pulses used in PCM, a transient nucleation $I(x, y, t)$ rate is taken into account: the expected number of critical nuclei generated during dt and in an unit volume h^3 located at (x,y) is calculated by:

$$N(x, y, t) = I(x, y, t) \cdot dt \cdot h^3 \tag{3}$$

During the nucleation step, critical nuclei are introduced into individual cells randomly but with a mean formulation rate given by $N(x, y, t)$.

An ohmic model approach is used to simulate the electrical behavior of the PCM cell. The electro-thermal solver relies on the coupled system of partial differential equations formed by the current conservation equation and the heat transfer equation.

$$\nabla \cdot (-\sigma \nabla V) = 0 \tag{4}$$

The heat equation in the PCM material includes the energy exchange due to the latent heat of melting.

$$\rho C_p \frac{\partial T}{\partial t} + \nabla \cdot (-k_{th} \nabla T) = \sigma (\nabla V)^2 + L \frac{dh}{d\eta} \frac{\partial \eta}{\partial t} \tag{5}$$

where σ, ρ, C_p, k_{th} and L stand for the PCM electrical conductivity, density, heat capacity, thermal conductivity and latent heat of melting and h is a smooth interpolation function. For PCM, σ and k_{th} depend on η and T. More precisely, σ is implemented using a state variable with four possible values (crystal, liquid, amorphous with high or low electrical resistivity) and takes into account electronic switching. The amorphous phase is electrically in the off-state if the local electric field is lower than a threshold electric field (E_{th}) and switches to the on-state if the local electric field becomes higher than E_{th}. The system of previous equations is discretized using the Finite-Element method with the Partial Derivative Equations interface of COMSOL multiphysics®.

3. Measurement results

Our simulation work is part of a more extended work presented in [15] in which for the first time the control of conductance level in PCM cells by mean of a frequency modulation of progressive SET pulses is reported. In this context, the simulation work intends to explore crystallization mechanisms taking place during the application of successive set pulses. Regarding the electrical characterization part, we performed experiments on a GST-based PCM array. The memory array consists of 16kbit single bank built on 28 nm CMOS technology front end on 300 mm wafer. The selector devices are MOS transistors with thin oxide. The PCM resistor is a GST225 PCM device integrated into the LETI Memory Advanced 300 mm Demonstrator (Fig. 1). The electrical measurements were carried out with an Agilent B1530 [15]. First a reset pulse is applied with the following characteristics: I_{Reset} = 557 µA and 20 ns\500 ns\20 ns (rise\width\fall times), which leads to a full reset state ($R > 10^6$ Ω). Next a train of successive pulses 20 ns\ 10 µs \20 ns (rise\width\fall times) were delivered to the cell. The selector gate is used to control the current. After each pulse the conductivity is dynamically measured at low field (V_{Read} = 0.2 V). If multiple read operations are carried out during the period between two set pulses, it is proven experimentally that drift lowers the conductance during this period [15].

Table 1
Thermal boundary resistances values.

TBR between heater and SiN	$5 \cdot 10^{-9}$ Km^2 W^{-1}
TBR between heater and GST	$2 \cdot 10^{-8}$ Km^2 W^{-1}
TBR between GST and SiN	$5 \cdot 10^{-9}$ Km^2 W^{-1}
TBR between GST and TiN	$2 \cdot 10^{-8}$ Km^2 W^{-1}

We studied two regimes: a high current regime (I_h = 160 µA) and a low current (I_l = 25 µA). After each pulse, the resistance of different 10 devices is averaged and plotted in Fig. 2. As can be seen the conductance (G) increases firstly linearly (pulses < 20–30) and then saturates when additional pulses are applied. This can be partially explained by the drift of the amorphous phase that happens during the period between successive set pulses.

4. Simulation results and discussion

Due to the small dimension of the heater in the lateral direction (5 nm) in comparison with its depth (45 nm) as visible on Fig. 1b, we assume two-dimensional simulations are a good compromise between precision and CPU time. The 2D domain used for the simulation including the different materials is depicted in Fig. 3. The phase field method which relies on a smooth interface representation requires a mesh size of 0.5 nm in the PCM domain. The resolution relies on two different meshes: a coarse mesh for the whole domain where the electro-thermal problem is solved and a finer mesh for the PCM domain where the PFM is solved.

Interfaces between materials become increasing important when the dimensions involved are of the tens nanometer scale [16]. Consequently we introduced TBR at the interfaces between heater and PCM, heater and encapsulating SiN and between PCM layer and encapsulating SiN as indicated on Fig. 3. The values used for the TBR given in Table 1 rely on published experimental results [16,17] .

Starting from a device with an amorphous dome obtained by the reset pulse simulation, we have qualitatively reproduced the progressive increase of conductance associated to low and high current set

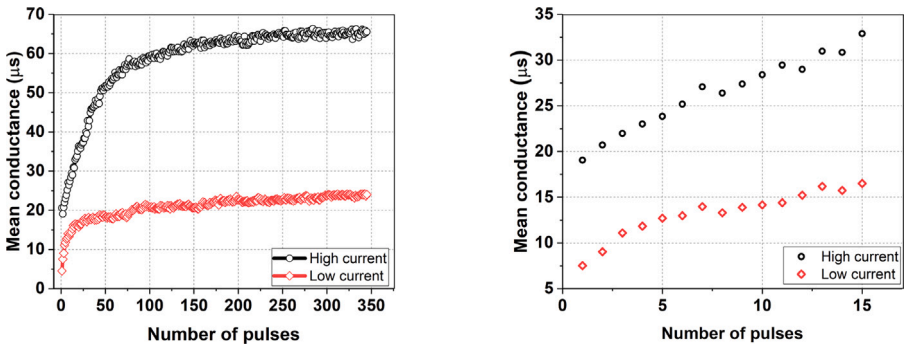

Fig. 2. G versus number of pulses — left: for 350 pulses — right: for the first fifteen pulses.

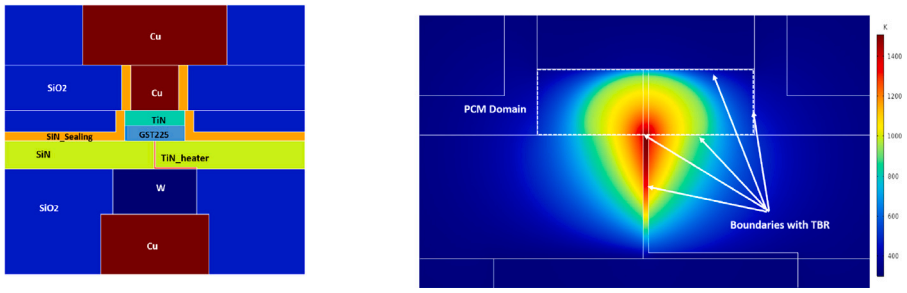

Fig. 3. Left: simulation domain — right: simulated temperature field during the plateau of the reset pulse including TBR localization.

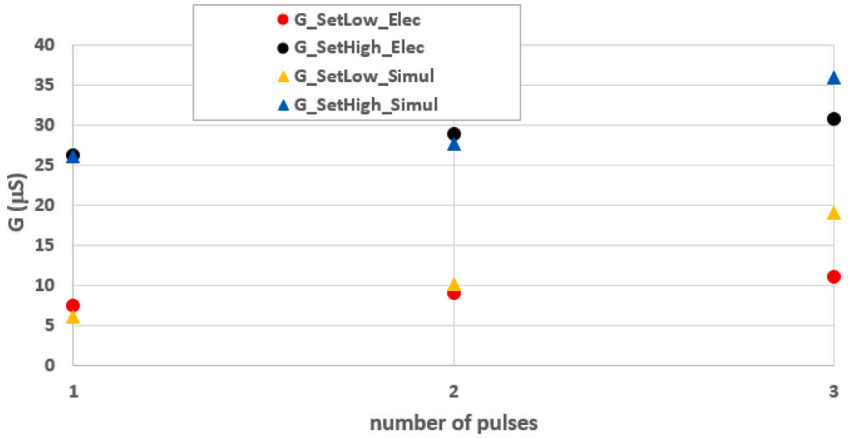

Fig. 4. Comparison of G by simulation versus electrical characterization for the three first pulses.

pulses. The mechanisms of recrystallization can be nucleation or growth dominated depending on the set pulse characteristics. Our simulations clearly indicate a nucleation dominated mechanism in the conditions of our set pulses. As plotted in Fig. 4, the increase of conductance associated to each set pulse is reproduced by the simulation for the three first pulses. For more pulses, the simulation model overestimates the increment of conductance because currently it does not integrate the drift phenomenon which is supposed to counterbalance the increase of conductance [15].

For the set pulse with $I = 25$ µA, neither fusion nor re-amorphization occurs during the set pulse and increase of conductance is due to nucleation and growth within the amorphous dome as illustrated by Fig. 5b. We hypothesize that the conductivity saturation can still be ascribed to the counter effect of drift even though no-reamorphization occurs. For the set pulse with $I = 160$ µA, the scenario of recrystallization is different because the current is high enough to trigger the melting of the central part of the active domain leading to a nucleation rate maximal in the periphery of the melted domain as visible in Fig. 6. As indicated by the simulation (Fig. 5c), the high current regime corresponds to a re-amorphization of the GST mushroom core, while the surrounding GST slowly nucleates, leading to the increase of conductance. It can be shown that in this scenario, the conductivity saturation can be fully explained by the counter effect of resistance drift of the amorphous, which tends to lower the conductance after each pulse [15].

In both set high and set low regimes, the temperature field obtained in the vicinity of the crystal/amorphous interface is not favorable to the regrowth of the interface excepted in a small part of the interface in the top of the amorphous domain. The simulations show that, if the current

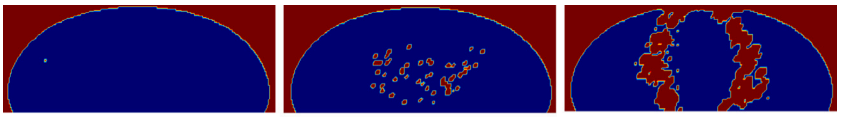

(a) after Reset pulse (b) 2^{nd} pulse I=25μA (c) 2^{nd} pulse I=160μA

Fig. 5. Progress of crystallization after 1000 ns for the second pulse: crystalline phase (purple red), amorphous phase (blue). (For interpretation of the references to color in this figure legend, the reader is referred to the web version of this article.)

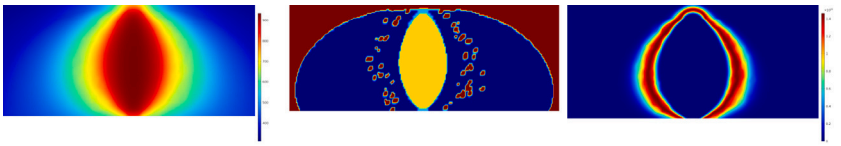

(a) Temperature (b) Phase (c) Nucleation Rate

Fig. 6. Pulse set I = 160 μA t = 600 ns - (b) the yellow domain corresponds to the melted PCM - (c) nucleation rate is maximal on the periphery of the melted domain. (For interpretation of the references to color in this figure legend, the reader is referred to the web version of this article.)

is high enough, each pulse causes the re-amorphization of a central GST dome core. So we can consider the drift is the same between two consecutive pulses whatever its rank in the train of pulses. As we assume that the conductivity drift after each pulse is identical pulse after pulse, a model linking the conductance increase, δG to the drift could be proposed (δG is due to the additional crystallization between two pulses); this model is presented and discussed in [15].

5. Conclusion

The progressive crystallization that occurs during the successive application of set pulses was studied by electrical characterization and simulation. Insight on the real mechanisms of crystallization is obtained by coupling Joule heating, diffusion of heat and a phase change model. We reproduce and explain the two different regimes of recrystallization corresponding to set low and set high pulses evidenced by electrical characterization. Thanks to this model the hypothesis that drift counterbalances the increase of conductance during the progressive application of set pulses is confirmed. This work paves the way to a better control of the set pulses to be used to generate predefined conductance levels in PCM devices for neuromorphic computing.

Declaration of competing interest

The authors declare that they have no known competing financial interests or personal relationships that could have appeared to influence the work reported in this paper.

Data availability

The authors do not have permission to share data.

Acknowledgments

This work was partially supported by the CEA NUMERICS program, which has received funding from the European Union's Horizon 2020 research and innovation program under the Marie Sklodowska-Curie grant agreement No 800945. It was also supported by the MeM-Scales EU Horizon 2020 research and innovation program under the grant agreement NO 871371.

References

[1] Wright CD. Beyond von-Neumann computing with nanoscale phase change memory devices. Adv Funct Mater 2013;23(18):2248–54. http://dx.doi.org/10.1002/adfm.201202383.
[2] Nandakumar SR. A phase change memory model for neuromorphic computing. J Appl Phys 2018;124(15). http://dx.doi.org/10.1063/1.5042408.
[3] Sebastian A. Computational phase-change memory: beyond von Neumann computing. J Phys D: Appl Phys 2019;52(44). http://dx.doi.org/10.1088/1361-6463/ab37b6.
[4] Demirag Y. PCM-trace: Scalable synaptic eligibility traces with resistivity drift of phase-change materials. In: Proceedings of ISCAS. 2021, http://dx.doi.org/10.1109/ISCAS51556.2021.9401446.
[5] Cueto O. Coupling the Phase-Field Method with an electrothermal solver to simulate phase change mechanisms in PCRAM cells. In: Proceedings of SISPAD. 2015, http://dx.doi.org/10.1109/SISPAD.2015.7292319.
[6] Karma Alain. Phase-field model of eutectic growth. Phys Rev E 1994;49(3):2245–50. http://dx.doi.org/10.1103/PhysRevE.49.2245.
[7] Plapp Mathis. Phase-field modelling of solidification microstructures. J Indian Inst Sci 2016;96:179–98.
[8] Henry Hervé. Orientation-field model for polycrystalline solidification with a singular coupling between order and orientation. Phys Rev B 2012;86(5):054117. http://dx.doi.org/10.1103/PhysRevB.86.054117.
[9] Tabatabaei Fatemeh. Phase field modeling of rapid crystallization in the phase change material AIST. J Appl Phys 2018;122. http://dx.doi.org/10.1063/1.4996429.
[10] Dhas Bensingh. A phase-field damage model for orthotropic materials and delamination in composite laminates. J Appl Mech 2018;85. http://dx.doi.org/10.1115/1.4038506.
[11] Min Lang. On realizing specific failure initiation criteria in the phase field model. Comput Methods Appl Mech Eng 2022;394. http://dx.doi.org/10.1016/j.cma.2022.114881.
[12] Prakash Ved. A phase-field model for thermo-mechanical fracture. Math Mech Solids 2022. http://dx.doi.org/10.1177/10812865221085198.
[13] Allen SM. A microscopic theory for antiphase boundary motion and its application to antiphase domain coarsening. Acta Metall 1979;27(6):1085–95. http://dx.doi.org/10.1016/0001-6160(79)90196-2.
[14] Kwon Y. Analysis of Intrinsic Variation of Data Retention in Phase-Change Memory Using Phase-Field Method. IEEE Electron Device Lett 2013;34(3):411–3. http://dx.doi.org/10.1109/LED.2013.2242038.
[15] Trabelsi A. Frequency modulation of conductance level in PCM device for neuromorphic applications. In: IEEE Proceedings of ESSCIRC. 2022, http://dx.doi.org/10.1109/ESSCIRC55480.2022.9911461.
[16] Reifenberg JP. Thermal boundary resistance measurements for phase-change memory devices. IEEE Electron Device Lett 2010;31(1):56–8. http://dx.doi.org/10.1109/LED.2009.2035139.
[17] Battaglia JL. The use of photothermal techniques for thermal conductivity and thermal boundary resistance measurments of phase-change chalcogenides alloys. J Appl Phys 2021;129. http://dx.doi.org/10.1063/5.0020983.